Article

A theoretical study and numerical simulation of a quasi-distributed sensor based on the low-finesse Fabry-Perot interferometer: Frequency-division multiplexing

José Trinidad Guillen-Bonilla[1,2], Alex Guillen Bonilla[3], Verónica M. Rodríguez Betancourtt[4], Héctor Guillen Bonilla[4], Antonio Casillas Zamora[1]

1 Computing and Electronic Departments, Centro Universitario de Ciencias Exactas e Ingenierías (CUCEI), University of Guadalajara, Blvd. M. García Barragán 1421, Guadalajara, Jalisco 44410, México; e-mail: **trinidad.guillen@academicos.udg.mx**; **antonio.czamora@academicos.udg.mx**;

2 Mathematic Department, Centro Universitario de Ciencias Exactas e Ingenierías (CUCEI), University of Guadalajara, Blvd. M. García Barragán 1421, Guadalajara, Jalisco 44410, México; e-mail:

3 Departamento de Ciencias Computacionales, Centro Universitario de los Valles, Universidad de Guadalajara, Ameca Km 45.5, C.P. 46600, Ameca, Jalisco, México. Ameca, Jalisco, México. e-mail: **alex.guillen@profesores.valles.udg.mx**

4 Materials Science Graduate School, Centro Universitario de Ciencias Exactas e Ingenierías (CUCEI), University of Guadalajara, Blvd. M. GarcíaBarragán 1421, Guadalajara, Jalisco 44410, México. E-Mails: **verónica.rodriguez@red.cucei.udg.mx**; **hectorguillenbonilla@gmail.com**

* Correspondence: **trinidad.guillen@academicos.udg.mx** Tel.: 01 (33) 13 78 59 00 ext. 27655

Abstract: The application of the sensors optical fiber in the areas of scientific instrumentation and industrial instrumentation is very attractive due to its numerous advantages. In the industry of civil engineering for example, quasi-distributed sensors made with optical fiber are used for reliable strain and temperature measurements. Here, a quasi-distributed sensor in the frequency domain is discussed. The sensor consists of a series of low-finesse Fabry-Perot interferometers where each Fabry-Perot interferometer acts as a local sensor. Fabry-Perot interferometers are formed by pairs of identical low reflective Bragg gratings imprinted in a single mode fiber. All interferometer sensors have different cavity length, provoking the frequency-domain multiplexing. The optical signal represents the superposition of all interference patterns which can be decomposed using the Fourier transform. The frequency spectrum is analyzed and sensor´s properties were defined. Following, a quasi-distributed sensor was numerically simulated. Our sensor simulation considers sensor properties, signal processing, noise system and instrumentation. The numerical results show the behavior of resolution vs. signal-to-noise ratio. From our results, the Fabry-Perot sensor has high resolution and low resolutions. Both resolutions are conceivable because the FDPA algorithm elaborates two evaluations of Bragg wavelength shift.

Keywords: Quasi-distributed sensor; Low-finesse Fabry-Perot interferometer; Sensor simulation; Frequency-domain multiplexing and resolution vs. signal-to-noise ratio.

---

1. Introduction

Bragg grating has a very particular peak in its reflection spectrum, that one is centered at the Bragg wavelength $\lambda_{BG} = 2n\Lambda$ [1]: Λ is the grating pitch and n is the effective fiber refraction index. The operational principle of fiber Brag grating sensor is based on the spectral shift of the central Bragg wavelength due to the variation of the pitch and refraction index because the temperature or strain

Preprints (www.preprints.org) | NOT PEER-REVIEWED | Posted: 3 April 2017 doi:10.20944/preprints201704.0001.v1

Peer-reviewed version available at *Sensors* **2017**, *17*, , 859; doi:10.3390/s17040859

change on the grating. The monitoring system needs to detect the wavelength shift with very high resolution, permitting its correct evaluation. This shift is evaluated from optical measurements, for example: a dual-OFC FBG interrogation system [2], tunable Fabry-Perot filter with a piezoelectric actuator [3] and direct spectroscopic detection [4].

Bragg gratings play an important role in the fiber-optic sensor technology. Such sensors are very attractive for quasi-distributed sensing employing only one optical fiber with many gratings printed along a fiber length. The conventional Bragg grating sensors use a broadband light source and a direct spectrometric detection technique. Its principal problem concerns to the detection of relatively small shifts in resonant wavelength of gratings array exposed to the strain or slow temperature changes. An additional application of Bragg gratings in sensor technology is to build interferometers within the single path fiber. In this case, Bragg gratings act as selective mirrors. The positions of gratings along the fiber length define the optical path difference. Frequency-division multiplexing, wavelength-division multiplexing and time-division multiplexing can be implemented [5-12].

The twin-grating fiber optic sensor was used for the temperature measurement. The optical sensor acts as a low-finesse Fabry-Perot interferometer and it consists of two identical Bragg gratings separated by a short distance. The Fourier Domain Phase Analysis (FDPA) algorithm was used for its signal demodulation. The FDPA algorithm evaluates the Bragg wavelength shift at the frequency domain. The algorithm is based on the evaluation of the phase of the interference pattern produced by light reflected from both gratings and on the determination of the Bragg wavelength shift. The wavelength shift sensitivity was measured to 0.00985nm/^{o}C [13]. This fiber sensor was also used for the measurement of static strain. Resolution of 0.2 μm/m was reported [14].

In reference [15], a quasi-distributed sensor was experimentally proposed. Twin-grating sensors were applied as local sensors. Frequency-division multiplexing was implemented. Following, in reference [16] this quasi-distributed sensor was described. The authors gave the next description: Frequency-division multiplexing was applied. A tunable external cavity diode laser was used for the sensor interrogation. The sensing systems consisted of a serial array of 14 twin grating sensors. All Bragg gratings had the same length of 0.5 mm and reflectivity of 0.8%. The Bragg wavelength of all gratings was 1550.6nm. The cavities were into the interval of 2 mm to 34 mm. The optical spectrum was acquired. Their frequency components were separated applying the fast Fourier transform (FFT) algorithm. There were 14 channels. Each channel was generated from each Fabry-Perot sensor. Another quasi-distributed fiber optic sensors can be found in references [17-22].

Under our knowledge, the quasi-distributed sensor described in Ref. [16] does not have an analytic analysis. Therefore, local sensor limitations are not known. Here, a theoretical analysis and numerical simulation is elaborated for the quasi-distributed sensor described in reference [16]. A broadband light source, direct spectrometric detection technique and frequency-domain multiplexing are considered in our study. Knowing its operation principle, the optical spectrum was represented mathematically. We analyzed the optical signal and then the quasi-distributed sensor´s properties were defined, for example: minimum and maximum cavities, number of samples, spatial resolution and multiplexing capability of a twin-grating fiber sensor. All parameters are expressed in terms of physical parameters and instrumentation characteristics. Following, the quasi-distributed sensor was numerically simulated (in operation) and we obtain the graph of Demodulation errors vs. signal-to-noise ratio. From our numerical results, the cavity length augments the resolution, all Fabry-Perot sensors have two resolutions: a high resolution and low resolution. The cavity length, low resolution and noise system define the transition between both resolutions. In general, our theoretical analysis and numerical simulation permit its optimal implementation and its design.

2. Optical signal

Fig. 1 shows our optical sensing system schematically. The optical system consists of a broadband source, an optical circular 50/50, an optical analyzer spectrometer (OSA spectrometer), a personal computer and a quasi-distributed sensor. The quasi-distributed sensor can be implemented by using a serial array of low-finesse Fabry-Perot interferometers [15,16]. The local sensors are formed by pairs of identical low reflective Bragg gratings imprinted in a single mode fiber. Each Fabry-Perot

Preprints (www.preprints.org) | NOT PEER-REVIEWED | Posted: 3 April 2017 doi:10.20944/preprints201704.0001.v1

Peer-reviewed version available at Sensors 2017, 17, , 859; doi:10.3390/s17040859

interferometer has a unique optical path length, obtaining the frequency-division multiplexing (FDM). The Bragg gratings have approximately the same length and typical reflectivity of 0.1%. Thus, wavelength-division multiplexing was eliminated for our optical sensor.

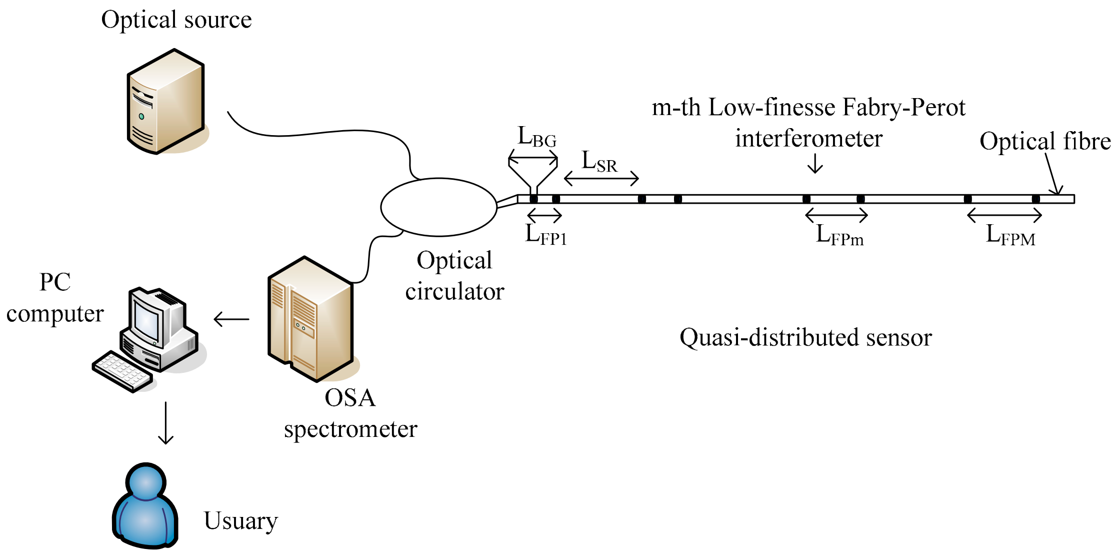

Figure 1. Sensing system

2.1. $\boldsymbol{R_T(\lambda)}$ and $\boldsymbol{R_T(\nu)}$ spectrums

When the quasi-distributed sensor does not have external perturbations, the optical signal $R_T(\lambda)$ will be the superposition of all interference patterns,

$$R_T(\lambda) = \sum_{m=1}^{M} R_m(\lambda) = R_1(\lambda) + R_2(\lambda) + R_3(\lambda) + \cdots + R_M(\lambda) \tag{1}$$

$R_T(\lambda)$ is the optical signal detected by the OSA spectrometer and $R_1(\lambda), R_2(\lambda), R_3(\lambda) \ldots R_N(\lambda)$ are interference patterns generated by all interferometer sensors. Considering the physical parameters, the optical signal can be re-written as [13]

$$R_T(\lambda) = \sum_{m=1}^{M} 2a_m \left[\left(\frac{\pi n_1 L_{BG}}{\lambda_{BG}}\right)^2 sinc^2\left(\frac{2n_1 L_{BG}(\lambda - \lambda_{BG})}{\lambda_{BG}^2}\right)\right]\left[1 + cos\left(\frac{4\pi n L_{FPm}(\lambda - \lambda_{BG})}{\lambda_{BG}^2}\right)\right] \tag{2}$$

where λ is the wavelength, a_m are amplitude factors, n_1 is the amplitude of the effective refractive index modulation of the gratings, L_{BG} is the length of gratings, λ_{BG} is Bragg wavelength, n is the effective index of the core, L_{FPm} is the mth cavity length and M is the number of low-finesse Fabry-Perot interferometers (local sensors). Analyzing the optical signal (2), all interference patterns have a similar enveloped function, the enveloped is the reflection spectrum of the gratings, the width Δ_{BG} is defined as the spectral distance between its +1 and -1 zeros,

$$\Delta_{BG} = \frac{\lambda_{BG}^2}{n_1 L_{BG}} \tag{3}$$

Each interference pattern has its own frequency component. There are M modulate functions where the frequency component ν_{FPm} will be

$$\nu_{FPm} = \frac{2nL_{FPm}}{\lambda_{BG}^2} \tag{4}$$

To know the frequency components, we apply the Fourier transform to optical signal

$$R_T(\nu) = \mathcal{F}\{R_T(\lambda)\} = \int_{-\infty}^{\infty} R_T(\lambda) e^{-i2\pi\nu\lambda} d\lambda \tag{5}$$

$R_T(\nu)$ is the frequency spectrum, $\mathcal{F}\{\ \}$ is the Fourier operator and ν is the frequency. Substituting Equs. (2), (3) and (4) into Equ. (5), the frequency spectrum is

$$R_T(\nu) = \int_{-\infty}^{\infty} \sum_{m=1}^{M} 2a_m \left[\left(\frac{\pi n_1 L_{BG}}{\lambda_{BG}}\right)^2 sinc^2\left(\frac{\lambda-\lambda_{BG}}{\Delta_{BG}}\right)\right]\left[1+cos\left(2\pi\nu_{FPm}(\lambda-\lambda_{BG})\right)\right] e^{-i2\pi\nu\lambda} d\lambda \tag{6}$$

Invoking the convolution properties and Fourier operator, we have

$$R_T(\nu) = \mathcal{F}\left\{\left[\left(\frac{\pi n_1 L_{BG}}{\lambda_{BG}}\right)^2 sinc^2\left(\frac{\lambda-\lambda_{BG}}{\Delta_{BG}}\right)\right]\right\} \otimes \mathcal{F}\left\{\sum_{m=1}^{M} 2a_m\left[1+cos\left(2\pi\nu_{FPm}(\lambda-\lambda_{BG})\right)\right]\right\} \tag{7}$$

the symbol $\otimes$ indicates the convolution. Using the identities: $cos^2(\varphi) = \frac{1}{2}\left(1+cos(2\varphi)\right)$, $cos(\varphi) = \frac{e^{i\varphi}+e^{-i\varphi}}{2}$, $\sum_{m=1}^{M} e^{-i\varphi_m} = \sum_{m=-M}^{-1} e^{i\varphi_m}$ and solving, the frequency spectrum $R(\nu)$ is

$$R_T(\nu) = \sum_{m=-M}^{M} R_m(\nu) = \sum_{m=-M}^{M} c_m tri\left(\frac{\nu-\nu_{FPm}}{\nu_{BG}}\right) \tag{8}$$

$R_T(\nu)$ spectrum is a set of triangle functions where c_m are amplitude factors, ν_{BG} is the bandwidth

$$\nu_{BG} = \frac{4n_1 L_{BG}}{\lambda_{BG}^2} \tag{9}$$

and ν_{FPm} are the center position of each triangle function. Here, all frequency components were separated as Fig 2 illustrates

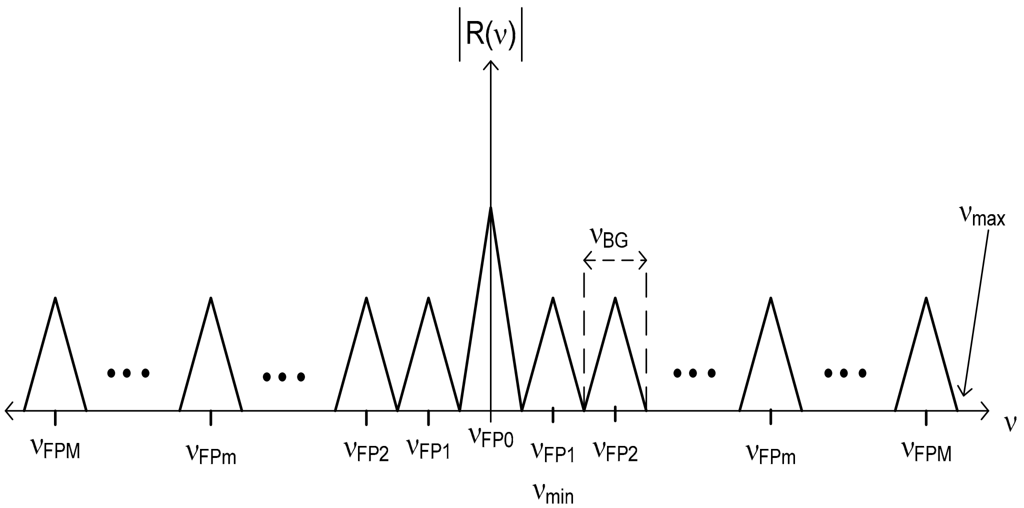

Figure 2. $R(\nu)$ frequency spectrum

2.2. $\boldsymbol{R_T(\lambda, \delta\lambda)}$ *and* $\boldsymbol{R_T(\nu, \delta\lambda)}$ *spectrums*

When the quasi-distributed sensor has external perturbations, the measured (temperature or string) affects the gating period Λ, the refraction index n, the length of gratings L_{BG} and cavity length L_{FPm} [13]. In turn, interference patterns has a small shift in response to a measured variation, the optical signal detected by the OSA spectrometer is

$$R_T(\lambda,\delta\lambda) = \sum_{m=1}^{M} 2a_m \left[\left(\frac{\pi n_1 L_{BG}}{\lambda_{BG}}\right)^2 sinc^2\left(\frac{2n_1 L_{BG}(\lambda-\lambda_{BG}-\delta\lambda_{BGm})}{\lambda_{BG}^2}\right)\right]\left[1+cos\left(\frac{4\pi n L_{FPm}(\lambda-\lambda_{BG}-\delta\lambda_{BGm})}{\lambda_{BG}^2}\right)\right] \quad (10)$$

The optical spectrum $R_T(\lambda,\delta\lambda)$ can be expressed as

$$R_T(\lambda,\delta\lambda) = \sum_{m=1}^{M} R_m(\lambda-\delta\lambda_{BGm}) = R_1(\lambda-\delta\lambda_{BG1}) + R_2(\lambda-\delta\lambda_{BG2}) + \cdots + R_M(\lambda-\delta\lambda_{BGM}) \quad (11)$$

where $R_T(\lambda,\delta\lambda)$ is the optical signal due to external perturbations and $\delta\lambda_{BGm}$ is Bragg wavelength shift due to measured change. Now, we estimate their frequency components through

$$R_T(\nu,\delta\lambda) = \mathcal{F}\{R_T(\lambda,\delta\lambda)\} = \int_{-\infty}^{\infty}\sum_{m=1}^{M} R_m(\lambda-\delta\lambda_{BGm})\, e^{-i2\pi\nu\lambda} d\lambda \quad (12)$$

Invoking the shift property and solving, the Fourier transform is

$$R_T(\nu,\delta\lambda) = \sum_{m=-M}^{M} R_m(\nu) e^{-i2\pi\nu\delta\lambda_{BGm}} \quad (13)$$

Observing the Equ. (13), the frequency spectrum $R_T(\nu,\delta\lambda)$ is the multiplication between $R_T(\nu)$ (Ecq. 8) and a set of phases. Those phases contain the information about the perturbations.

3. Cavity length

For all quasi-distributed sensors based on interferometers (optical fibre), the cavity length is a very important parameter since it defines the sensor characteristics. Their limits depend of instrumentation, local sensor characteristics and signal demodulation. Following, we determine minimum and maximum cavities where the low-finesse Fabry-Perot interferometer can be applied.

3.1. Minimum cavity length

The Fourier Domain Phase Analysis (FDPA) algorithm was developed for the twin-grating fiber optic sensor [13]. This algorithm does not accept additional information and does not accept the loss information, therefore, good signal detection and good frequency component identification are necessary. From Fig. 2, first frequency components ν_{FP1} can be defined by

$$\nu_{FP1} = \nu_{BG} \quad (14)$$

The condition (14) eliminates the overlapping between components, ν_{FP1} and ν_{FP0}. Using the Equs. (4) and (9), we have

$$\frac{2nL_{FP1}}{\lambda_{BG}^2} = \frac{4n_1 L_{BG}}{\lambda_{BG}^2} \quad (15)$$

As $n_1 \approx n$, the minimum cavity length will be

$$L_{FP1} = 2L_{BG} \quad (16)$$

It´s not possible smaller cavities because the FDPA algorithm can not demodulate the optical signal.

3.2. Maximum cavity length

The optical sensing system applies the direct spectroscopic detection [4]. This technique uses an optical spectrometer analyzer which defines the maximum cavity length L_{FPM}. The OSA spectrometer has a limit for the optical signal detection. The limit is the Full-With Half-Maximum (FWHM). Considering the sampling theorem, the OSA spectrometer can detect the signal if and only if next condition is true,

$$\Delta\lambda_{\mathrm{FPmin}} = 2\Delta\lambda \quad (17)$$

Preprints (www.preprints.org) | NOT PEER-REVIEWED | Posted: 3 April 2017 doi:10.20944/preprints201704.0001.v1

Peer-reviewed version available at Sensors 2017, 17, , 859; doi:10.3390/s17040859

where $\Delta\lambda_{\mathrm{FPmin}}$ is the minimum period detectable (FWHM) and $\Delta\lambda$ is its spectrometer resolution. Then, the maximum frequency component can be expressed as

$$\nu_{FPM} = \frac{1}{\Delta\lambda_{\mathrm{FPmin}}} \tag{18}$$

From Fig. 2 and Equ. (4), last frequency component ν_{FPM} can be determined by

$$\nu_{FPM} = \frac{2nL_{FPM}}{\lambda_{BG}^2} \tag{19}$$

Combining Equs. (17), (18) and (19), the maximum cavity length is

$$L_{FPM} = \frac{\lambda_{BG}^2}{4n\Delta\lambda} \tag{20}$$

Equ. (20) indicates the maximum cavity length where OSA spectrometer can detect the optical signal. It´s not possible bigger cavities because the instrumentation can not detect the optical signal. Using Equs. (16) and (20), the cavity length can be into the interval of

$$2L_{BG} \leq L_{FP} \leq \frac{\lambda_{BG}^2}{4n\Delta\lambda} \tag{21}$$

4. Capacity of frequency-division multiplexing

In the quasi-distributed sensor, each low-finesse Fabry-Perot interferometer generates an interference pattern and then each pattern produces a channel in the frequency domain. The enveloped function produces the bandwidth ν_{BG} and the modulate function provokes the frequency components: $-\nu_{FPm}$, ν_{FP0} and ν_{FPm}. The term ν_{FP0} contains information from all Fabry-Perot interferometers while $-\nu_{FPm}$ and ν_{FPm} contain similar information from the mth Fabry-Perot sensor. From Fig. 2, we have the next condition

$$M = \frac{\nu_{FPM}}{\nu_{FP1}} \tag{22}$$

In other words, the capacity of frequency-division multiplexing M is given by the relation between last and first frequency components. Substituting the Equs. (14), (15) and (17) into (22), the capacity M can be re-written as

$$M = \frac{L_{FPM}}{L_{FP1}} \tag{23}$$

Finally, substituting the Equs. (16) and (20) into Equ. (22), we have

$$M = \frac{\lambda_{BG}^2}{8nL_{BG}\Delta\lambda} \tag{24}$$

This expression gives the limit for the multiplexing capacity within one wavelength channel.

4. Number of samples

When the optical spectrometer analyzer instrument acquires the optical signal, the reflection spectrum is recorded as a series of digital samples. If a minimum and maximum wavelengths within a working interval $\lambda_w = \lambda_{max} - \lambda_{min}$: λ_{max} is the maximum wavelength, λ_{min} is the minimum wavelength and $\delta\lambda$ is the wavelength step. The signal samples $R_T(\lambda_k)$ are taken wavelengths $\lambda_k = \lambda_{min} + k\delta\lambda$ where $k = 0,1,2,\ldots,N-1$, N is the number of samples. The representation of such a signal in Fourier domain is also discrete. Therefore, we obtain next condition from Fig. 2

$$\nu_s \geq 2\nu_{max} = 2\left(\nu_{FPM} + \frac{\nu_{BG}}{2}\right) \tag{25}$$

where ν_{max} is the maximum frequency, ν_s is the sampling frequency and Nyquist theorem was considered. Substituting Equs. (9) and (19) into Equ. (25), we have

$$\nu_s \geq \frac{4n}{\lambda_{BG}^2}(L_{FPM} + 2L_{BG}) \tag{26}$$

Since $\nu_s = \frac{1}{\delta\lambda}$, we have

$$\delta\lambda \leq \frac{\lambda_{BG}^2}{4n(L_{FPM} + 2L_{BG})} \tag{27}$$

Finally, the number of sample is

$$\mathrm{N} = \frac{\lambda_w}{\delta\lambda} = \frac{4\lambda_w n(L_{FPM} + 2L_{BG})}{\lambda_{BG}^2} \tag{28}$$

The number of samples depends of optical system parameters.

5. Digital demodulation

The demodulation is the complete signal processing algorithm developed for quasi-distributed sensor based on the low-finesse Fabry-Perot interferometers. The complete processing algorithm combines the Fourier Domain Phase Analysis (FDPA) algorithm and a bank of M filters. The FDPA algorithm was described in Ref. [13] while the bank of filters is

$$\mathrm{F}(\nu) = rect\left(\frac{\nu}{\nu_{BG}}\right) \otimes \sum_{m=1}^{M} \delta(\nu - \nu_{FPm}) \tag{29}$$

where the symbol $\otimes$ indicates the convolution operation, the rect function has next definition

$$\mathrm{rect}(\nu) = \begin{cases} 1 & |\nu| < \dfrac{\nu_{BG}}{2} \\ 0 & |\nu| > \dfrac{\nu_{BG}}{2} \end{cases} \tag{30}$$

and δ is the Dirac delta. Invoking the Diract delta properties, the bank of M filters is

$$\mathrm{F}(\nu) = \sum_{m=1}^{M} rect\left(\frac{\nu - \nu_{FPm}}{\nu_{BG}}\right) \tag{31}$$

The bank filter of M filters is a series of rect function: ν_{FPm} is the central position and ν_{BG} is its bandwidth.

The digital demodulation consists of two phases: calibration and measurements. In the calibration, there are four steps: 1) $R_T(\lambda)$ is acquired, 2) $R_T(\nu)$ is computed, 3) $R_m(\nu)$ is filtered $R_m(\nu) = R_T(\nu)F(\nu)$ and 4) we calculate its complex conjugate $R_m^*(\nu)$ where * indicates complex conjugate. In the measurement, there are seven steps: 1) $R_T(\lambda, \delta\lambda)$ is acquired, 2) $R_T(\nu, \delta\lambda)$ is computed, 3) $\tilde{R}_m(\nu, \delta\lambda)$ is filtered $\tilde{R}_m(\nu, \delta\lambda) = R_T(\nu, \delta\lambda)F(\nu)$, 4) the relative phase φ_{rel} is calculated, 5) the ambiguity $2\pi P$ is eliminated and then absolute phase φ_{abs} is calculated and 6), 7) the Bragg wavelength shift is computed, a digital adaptive filter is applied [23].

Due to the presence of the noise in the original signal, the calculated phased will be fluctuating. To minimize the noise influence and provide the best estimate, the absolute phase is multiplied with a set of coefficients. Those coefficient act as an adaptive filter. The Fig. 3 illustrates the digital demodulation schematically.

Preprints (www.preprints.org) | NOT PEER-REVIEWED | Posted: 3 April 2017 doi:10.20944/preprints201704.0001.v1

Peer-reviewed version available at Sensors 2017, 17, , 859; doi:10.3390/s17040859

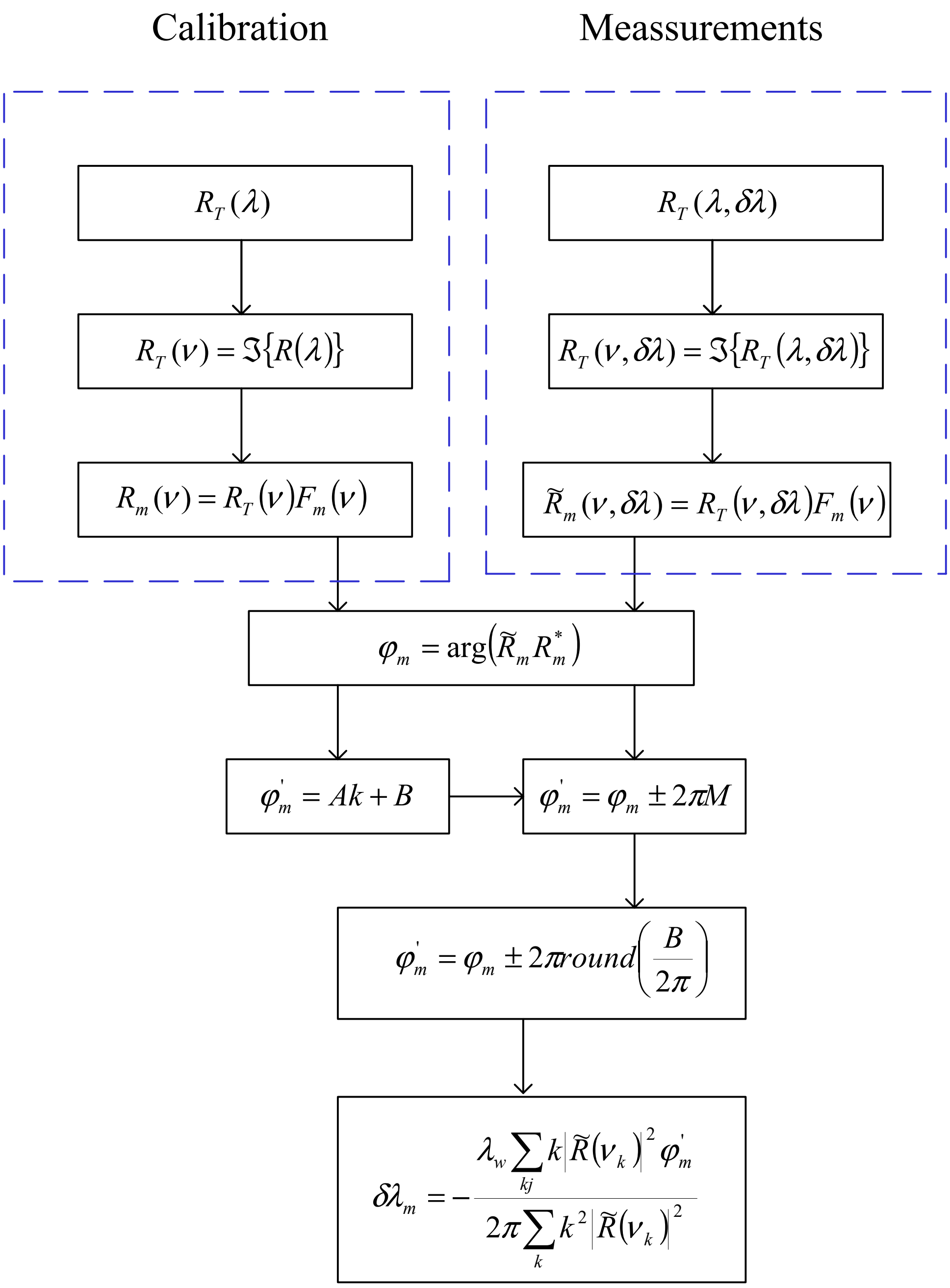

Figure 3. Digital demodulation represented schematically

6. Numerical simulation and discussion

6.1. Parameters and Results

To test and compare our theoretical analysis, we performed a numerical simulation of quasi-distributed sensor based on low-finesse Fabry-Perot interferometers. Three Fabry-Perot sensors were simulated. Their physical parameters can be observed on Table 1. Discrete spectrums were simulated using the physical parameters. Noise was simulated by adding, to those samples, pseudorandom numbers with Gaussian distribution, the interval was from $\sqrt{SNR} = 10^0$ to $\sqrt{SNR} = 10^4$. Typical of Bragg gratings with rectangular profile at refractive index modulation was used. In most of our numerical experiments, the number of samples was equal to 1024 (Fast Fourier transform algorithm was considered). For each local sensor, the reference spectrum and 50 measurements were simulated. The measurements were into the interval of, S1→0 to 0.2 nm, S2→0 to 0.4 nm and S3→0 to 0.7nm. Fig. 4 shows the spectrum $R_T(\lambda)$, Fig. 5 shows the spectrum $R_T(\nu)$ and Fig. 6 presents our numerical results: Demodulation errors vs SNR$^{1/2}$. A Laptop Toshiba 45C was used, their properties were 512 of RAM memory and velocity of 1.7 GHz.

Table 1. Quasi-distributed sensor parameters

Sensor number	Sensor parameters	Signal values
Low-finesse Fabry-Perot interferometer 1 (S1)	L_{FP1}=4 [mm] L_{BG}=0.5 [mm] n=1.46 $\lambda_{BG} = 1532.5$ [nm]	$\Delta\lambda_{BG} = 3.22$ [nm] (Equ. 3) $\nu_{FP1} = 4.95$ [Ciclos/nm] (Equ. 4) $\nu_{BG} = 1.23$[Ciclos/nm] (Equ. 9)
Low-finesse Fabry-Perot interferometer 2 (S2)	L_{FP2}=8 [mm] L_{BG}=0.5 [mm] n=1.46 $\lambda_{BG} = 1532.5$ [nm]	$\Delta\lambda_{BG} = 3.22$ [nm] (Equ. 3) $\nu_{FP2} = 9.91$[Ciclos/nm] (Equ. 4) $\nu_{BG} = 1.23$[Ciclos/nm] (Equ. 9)
Low-finesse Fabry-Perot interferometer 3 (S3)	L_{FP3}=16 [mm] L_{BG}=0.5 [mm] n=1.46 $\lambda_{BG} = 1532.5$ [nm]	$\Delta\lambda_{BG} = 3.22$ [nm] (Equ. 3) $\nu_{FP3} = 19.82$[Ciclos/nm] (Equ. 4) $\nu_{BG} = 1.23$[Ciclos/nm] (Equ. 9)

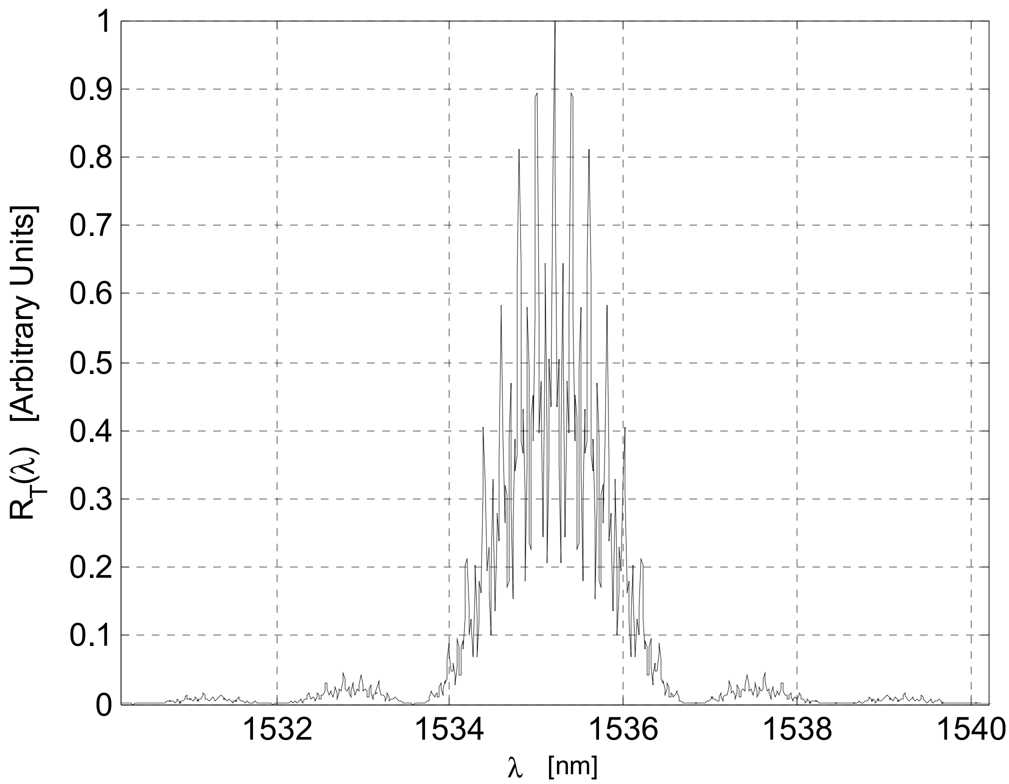

Figure 4. Optical signal $R_T(\lambda)$

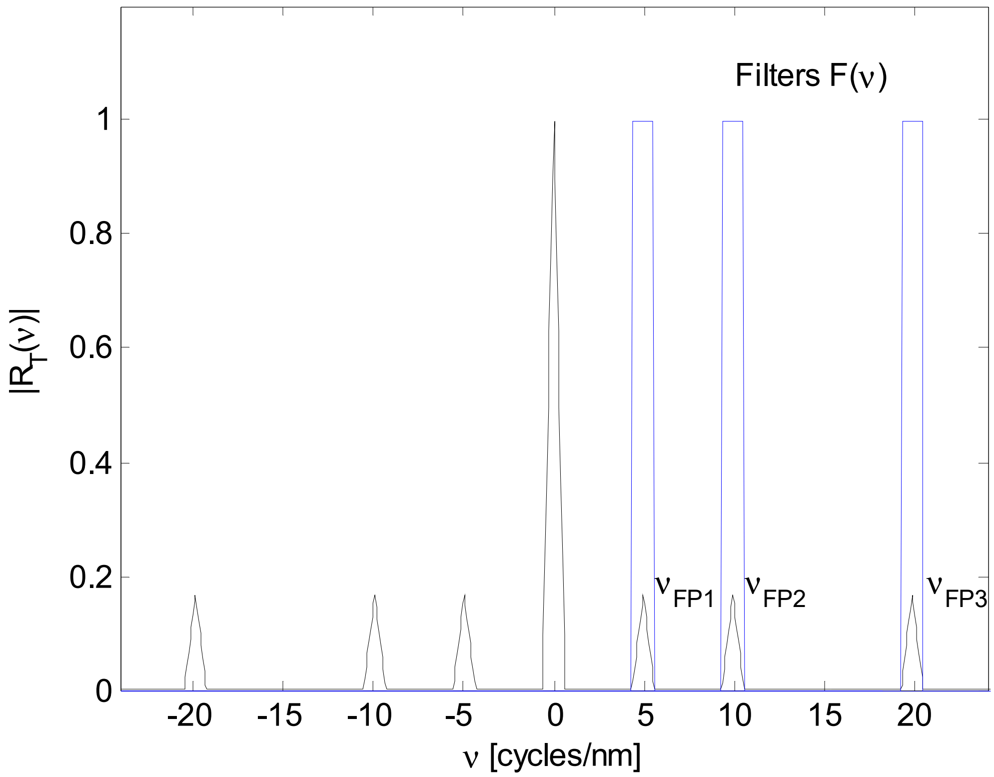

Figure 5. Optical signal $R_T(\nu)$

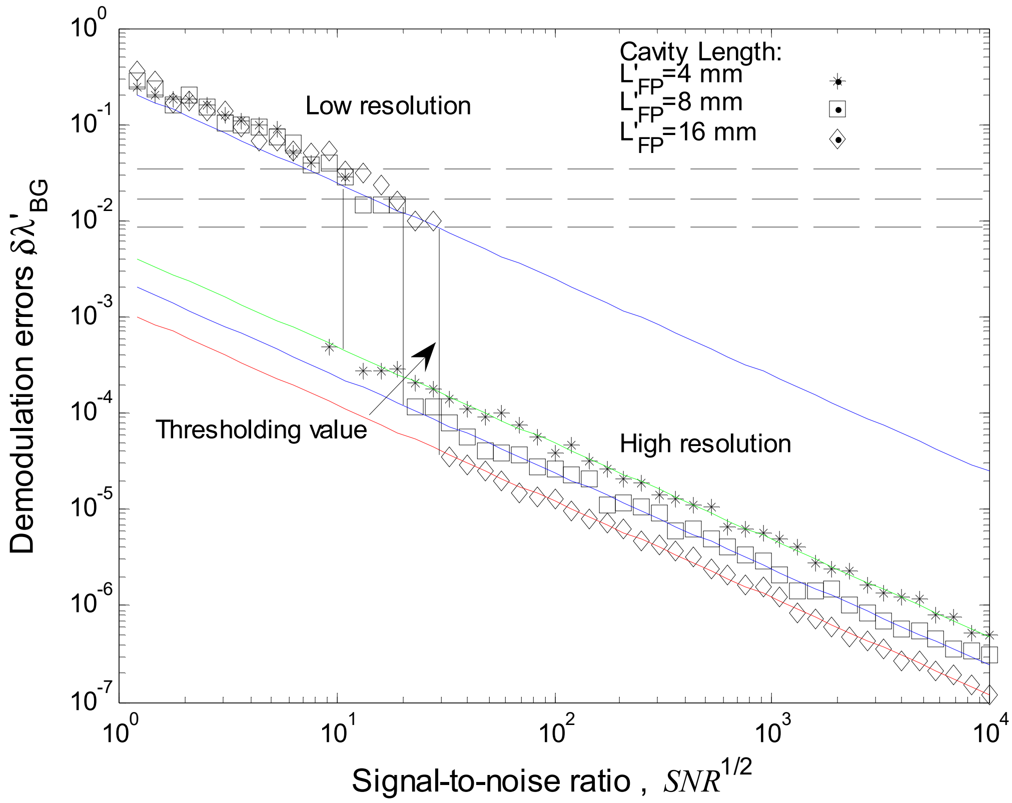

Figure 6. Numerical results

Preprints (www.preprints.org) | NOT PEER-REVIEWED | Posted: 3 April 2017 doi:10.20944/preprints201704.0001.v1

Peer-reviewed version available at *Sensors* **2017**, *17*, , 859; doi:10.3390/s17040859

If the OSA spectrometer has $\Delta\lambda = 10\ pm$ (typical value), the quasi-distributed sensor will have their limits as Table 2 illustrates.

Table 2. Quasi-distribuido sensor limits ($\Delta\lambda = 10pm$)

Parameters	Value	Equation
L_{FPmin}	1 [mm]	(Equ. 16)
L_{FPM}	40.2[mm]	(Equ. 20)
$L_{FPmin} \leq L_{FP} \leq L_{FPM}$	$1 \leq L_{FP} \leq 40$ [mm]	(Equ. 21)
M	40	(Equ. 23,24)
ν_{max}	102.47 [Ciclos/nm]	(Equ. 25)
ν_s	204.95 [Ciclos/nm]	(Equ. 26)

From Tables 1 and 2, the simulated quasi-distributed sensor satisfies the instrumentation and signal requirements. Observing Table 1 and Figures 4, 5, numerical results are in concordance with the theory. Thus, we confirm our theoretical analysis. Our numerical results can be observed at Fig. 6.

Fig. 6 shows the behavior Demodulation errors vs signal-to-noise rate $SNR^{1/2}$. If the demodulation error is denominated resolution then low-finesse Fabry-Perot has two resolutions: low resolution and high resolution. Two resolutions are possible because the FDPA algorithm dose two evaluations of Bragg wavelength shift [13,23]. All Fabry-Perot sensors have similar low resolution however each local sensor has its own high resolution. The high resolution depends of cavity length. If the cavity length is bigger then Fabry-Perot sensor will have better resolution.

6.2. Discussion

Based on our theoretical analysis and numerical simulation, the quasi-distributed sensor would be built on the low-finesse Fabry-Perot interferometer. Our theoretical analysis optimizes its implementation. Instrumentation, local sensor properties, noise (Gaussian distribution) and signal processing were considered. The quasi-distributed sensor has good sensitivity and excellent resolution. All Fabry-Perot sensors have two resolutions: low resolution and high resolution (See Fig. 6). Low resolution was obtained when Bragg wavelength shift was evaluated with enveloped function. High resolution was obtained when Bragg wavelength shift was evaluated combining the enveloped and modulate functions [13,23].

When the noise is big, signal-to-noise ratio (SNR) is small. In this case, the FDPA algorithm can not evaluate Bragg wavelength shift, causing the transition from high resolution until low resolution. That one can be observed at Fig. 6. As the signal is (necessary) into the interval of $-\pi$ to π and based on the signal detection theory, the thresholding value is

$$3\sigma_{env} < \frac{\Delta\lambda_{FPm}}{2} \tag{32}$$

where σ_{env} is the low resolution (resolution by enveloped function) and $\Delta\lambda_{FPm} = \frac{1}{\nu_{FPm}}$ is the period of our frequency component. The threshold divides between low and high resolutions. Substituting Equ. (4) into Equ. (32), we have

$$\sigma_{env} < \frac{\lambda_{BG}^2}{12nL_{FPm}} \tag{33}$$

From Equ. (33), each low-finesse Fabry-Perot interferometer has its own thresholding value. This one depends on the cavity length, Bragg wavelength and refraction index. For example: our Fabry-Perot sensors have next thresholding values, S1→0.033nm, S2→0.016nm and S3→0.008nm. The thresholding value is smaller if the cavity length is bigger.

In the quasi-distributed sensor, ghost interferometers are eliminated if the separation between any two interferometers satisfy the expression $L_{sp} > L_{FPM}$ where L_{sp} is the spatial resolution. If Fabry-Perot interferometers are formed by uniform unapodized gratings with equal length L_{BG}, the bandwidth of each peak is given by Equ. (9). To be separated in the frequency domain, two peaks should not overlap. This condition imposes the following constrains: the minimum distance between centers of gratings for the shortest interferometers is $2L_{BG}$ and the difference in the cavity lengths of any two Fabry-Perot interferometers must exceed $2L_{BG}$.

Our future research work has the next directions: Wavelength-division multiplexing (WDM) can be implemented based on the low-finesses Fabry-Perot interferometers. The theoretical resolution is another direction. Technical applications are possible, for example: temperature, strain, humidity, force measurement and oil detection.

7. Conclusions

The quasi-distributed optical fibre sensor based on the low-finesse Fabry-Perot interferometer, was studied theoretically and simulated numerically. Theory and simulation are in concordance. Our study considers quasi-distributed sensor properties, local sensor properties, signal processing, noise source, frequency-division multiplexing and instrumentation. Our numerical results showed that all Fabry-Perot sensors have two resolutions: low resolution and high resolution. Low resolution is similar for all sensors however each Fabry-Perot sensor has its own high resolution. The thresholding value (from high resolution to low resolution) was defined in terms of low resolution and physical parameters.

The quasi-distributed sensor has potential industrial applications, for example: structure monitoring, security system, humidity sensing and level sensing.

Acknowledgments: José Trinidad Guillen Bonilla thanks to CONACyT of Mexico by the scholarship. He also expresses your acknowledgments to S. V. Miridonov for your counseling and comments. This work was began at the CICESE and finished at the Guadalajara University.

Author Contributions: José Trinidad Guillen Bonilla performed the theoretical analysis and numerical simulation. A. Guillen corroborated the numerical simulation. All authors wrote the paper. All authors read and approved the final manuscript.

Conflicts of Interest: The authors declare no conflict of interest.

References

1. Kashyap R. Photosensitive Optical Fibers: Device and Applications. Optical Fiber Technology, **1994**, 1, 17-34. doi: 10.1006/ofte.1994.1003
2. Posada-Roman J. E.; Garcia-Souto J. A.; Poiana D. A. and Acedo P. Fast Interrogation of Fiber Bragg Gratins with Electro-Optical Dual Optical Frequency Combs. Sensors, **2016**, 16,2007. doi:10.3390/s16122007
3. Di Sante R. Fibre Optic Sensors for Structural Healt Monitoring of Aircraft Composite Structures: Recent Advances and Applications. Sensors, **2015**, 15, 18666-18713; doi:10.3390/s150818666
4. Miridonov S. V.; Shlyagin M. G.; and Spirin V. V. Resolution limits and efficient signal processing for fiber optic Bragg grating sensors with direct spectroscopic detection. Processing of Optical Measurements Systems for Industrial Inspection III, Vol. 5144, Munich, Germany, 23-26 June **2003**, Osten W.; Creath K.; Kujawiska M.
5. Ben Zaken B. B.; Zanzury T. and Maka D. An 8-Channel Wavelength MMI Demodultiplexer in Slot Waveguide Structures. Materials, **2016**, 9,881; doi:10.3390/ma9110881
6. Huang J.; Zhou Z.; Zhang L.; Chen J.; Ji C. and Pham T. Strain _Modal Analysis of Small and Light Pipes Using Distributed Fibre Bragg Grating Sensors. Sensors, **2016**, 16, 1583; doi:10.3390/s16101583
7. Weng Y.; Ip E.; Pan Z. and Wang T. Advances Spatial-Division Multiplex Measurement Systems Propositions-From Telecommunication to Sensing Applications: A Review. Sensors, **2016**, 16, 1387; doi:10.3390/s16091387
8. Ali T. A.; Shehata M. I. and Mohamed N. A. Design and performance investigation of a highly accurate apodized fiber Bragg grating-based strain sensors in single and quasi-distributed systems. Applied Optics, **2015**, Vol 16, Issue 16, 5243-5251; https://doi.org/10.1364/AO.54.005243

9. Cibula E. and Donlagic D. In-line short cavity Fabry-Perot strain sensor for quasi distributed measurements utilizing standard OTDR. Optic Express, **2007**, Vol. 15, No. 14, 8719-8730; https://doi.org/10.1364/OE.15.008719
10. Kežmah M. and Đonlagic. Multimode All-fiber quasi-distributed refractometer sensor array and cross-talk mitigation. Applied Optics, **2007**, Vol. 46, Issue 19, 4081-4091; htpps://doi.org/10.1364/AO.46.004081
11. Werzinger S.; Bergdolt S.; Engelbrecht R.; Torsten T. and Schmauss B. Quasi-Distributed Fiber Bragg Graint Sensing Using Steppen Incoherent Optical Frequency Domain Reflectometry. Journal of Lightwave Technology, **2016**, Vol. 34, Issue 22, 5270-5277;
12. Yu Z.; Yang J.; Yuan Y.; Li C.; Liang S.; Hou L.; Peng F.; Wu B.; Zhang J.; Liu Z. and Yuan L. Quasi-distributed birefringence dispersion measurement for polarization maintain device with hihj accuracy based on white light interferometry. Optic Express, **2016**, Vol. 24, No. 2, 1587-1597; DOI:10.1364/OE.24.001587
13. Miridonov S. V.; Shlyaing M. G. and Tentori D. Twin-grating fiber optic sensor demodulation. Optics Communications, **2001**, 191, 253-262.
14. Shlyagin M. G.; Swart P. L.; Miridonov S. V.; Chtcherbakov A. A.; Márquez Borbon I. and Spirin V. V. Static strain measurement with sub-micro-strain resolution and large dynamic range using a twin-Bragg.grating Fabry-Perot sensor. Optical Engineering, **2002**, 41(8), 1809-1814; doi:10.1117/1.1489048
15. Shlyagin M. G.; Miridonov S. V. and Tentori D. Frequency multiplexing of in-fiber Bragg grating sensors using tunable laser. Processing of Micro-optical for Measurement, Sensors, and Microsystems II and Optical Fiber Sensor Technologies and Applications, Vol. 3099, Munich, Germany, September 24, **1997**, 348; doi:10.1117/12.281246
16. Shlyagin M. G.; Miridonov S. V.; Márquez-Borbón I.; Spirin V. V.; Swart P. L. and Chtcherbakov A. A. Multiplexed twin Bragg grating interferometer sensor. Proceeding of Optical Fiber Sensors Conference Technical Digest, OFS 2002, 10 May **2002**, 191-194; doi:101109/OFS.2002.1000534
17. Trontz A.; Cheng B.; Zeng S.; Xiao H. and Dong J. Development of Metal-Ceramic Coaxial Cable Fabry-Perot Interferometer Sensors for High Temperature Monitoring. Sensors, **2015**, 15, 24914-24925; doi:10.3390/s151024914
18. Li X.; Sun Q.; Liu D.; Liang R.; Zhang J.; Wo J.; Shum P. P. and Liu D. Simultaneous wavelength and frequency encoded microstructure based quasi-distributed temperature sensor. Optics Express, **2012**, Vol. 20, No. 11, 12076-12084
19. Tao Y. J.; Ran Z. L. and Zhou C. X. Fiber-optic Fabry-Perot sensors based on a combination of spatial-frequency division multiplexing and wavelength division multiplexing formed by chirped fiber Bragg grating pairs. Applied Optics, **2006**, Vol. 45, Issue 23, 5815-5818; htpps:doi.org/AO.45.005815
20. Rao Y. J.; Henderson P. J.; Jackson D. A.; Zhang L. and Bennion I. Simultaneous strain, temperature and vibration measuremen using a multiplexed in-fibre-Bragg-grating/fibre-Fabry-Perot sensor system. Electronics Letter, **1997**, Vol. 33, No. 24, 2063-2064; doi:10.1049/el:19971409
21. Martinez-Manuel R.; Shlyagin M. G.; Miridonov S. V. and Meyer J. Vibration Disturbance Localization Using a Serial Array of identical Low-Finesse Fiber Fabry-Perot Interferometers. IEEE Sensors, **2012**, Vol. 12, Issue 1, 124-127; doi:10.1109/JSEN.2011.2119479
22. Viet Nguyen L.; Vasiliev M. and Alameh K. Three-wave Fiber Fabry-Perot Interferometer for Simultaneous Measurement of Temperature and Water Salinity of Seawater. IEEE Photonics Technology Letters, **2011**, Vol. 23, Issue 7, 450-452; doi: 10.1109/LTP.2011.2109057
23. Miridonov S. V.; Shlyaing M. G. and Tentori D. Digital demodulation of twin-grating fiber-optic sensor. Proceeding of Conference on Fiber Optic and Laser Sensor and Application, Vol. 3541, Boston, Massachsetts, USA, **1998**, 33-40.